Proceedings World Geothermal Congress 2000
Kyushu - Tohoku, Japan, May 28 - June 10, 2000

RESERVOIR SIMULATION STUDY OF THE ONIKOBE GEOTHERMAL FIELD, JAPAN

Shigetaka Nakanishi[1] and Nobuyuki Iwai[2]
[1]Electric Power Development Co., Ltd., 15-1, Ginza 6-Chome, Chuo-ku, Tokyo, 104-8165, Japan
[2]Kaihatsu Computing Service Center, Ltd., 2-18, Fukagawa 2-chome, Koto-ku, Tokyo, 135-8451, Japan

Key Words: Onikobe, Japan, numerical model, reservoir simulation, MINC

ABSTRACT

This paper presents the results of a numerical modeling effort to construct the mathematical model of the Onikobe reservoir with an improved quality, thereby permitting more accurate forecasts of reservoir performance, and facilitating efficient reservoir management. The steady "natural" state model of the field was developed by a natural state simulation. After the natural state model was derived by the trial and error matching of measured and calculated temperature and pressure distributions, a further calibration of the model was carried out by matching the known and calculated enthalpy histories of the existing wells. MINC (Multiple Interacting Continua) scheme to represent the naturally fractured reservoir was introduced to these history calculations, with equivalent steady properties. The thermal effects of reinjected water on the production wells could be reproduced by the simulation. These calculations indicate that the average fracture spacing of the reservoir nearby southern reinjection area was around 100m.

1. INTRODUCTION

The Onikobe geothermal field in the Miyagi prefecture in Japan has been developed and produced at a rated capacity of 12.5 MW, by the Electric Power Development Company (EPDC) since 1975. The Onikobe geothermal wellfield is shown in Fig.1. The 24-year performance history of the Onikobe reservoir involves two principal phenomenological characteristics. The first is the evolution of drilling practice to maintain field operations. All of the early production wells were vertical and completed in the "shallow" two phase reservoir, because strongly acidic fluids which were unsuitable for use in the plant were encountered at deeper levels during exploration (Abe, 1988). This early steam production was not sustainable, however, and steam production from the shallow reservoir declined with a continuous decline in enthalpy. The production in this field at present, however, comes from the "deep" reservoir developed several years later, and from deviated wells to the outside of the power station area. The changes in production/reinjection scheme also, in turn, affected the reservoir mass and heat flow characteristics. The second noteworthy characteristics of the reservoir production history involve significant temporal changes in geochemical compositions of the produced fluids. Temporal shifts in geochemistry have been observed corresponding to changes in the production/injection scheme and reflecting the significant spatial variation of the chemical compositions of the geothermal fluids in the reservoir. These changes appear to reflect the effects of both natural and artificial convection and rock/water interactions, downflows of meteoric surface waters into the underlying reservoir system, and mixing of concentrated reinjected brines into the ambient reservoir waters.

This paper presents the results of a numerical modeling effort to incorporate these production characters, in order to forecast reservoir performance in the future, and to perform proper reservoir management. Sanyal *et al.* (1990) have performed a numerical reservoir modeling study to verify if the production capacity could be increased from 12.5 MW to 25 MW at Onikobe. The historical data for "deep" production wells were available, however, only for 4 wells (Well 127, 128, 129 and 130) at that time. Since a number of production and reinjection make-up wells had been drilled since that time, and enough well production histories with sufficient duration were available for a history matching simulation to refine a reservoir model, we tried to construct a mathematical model of the Onikobe field with an improved quality.

In this modeling study, MINC scheme (Pruess and Narasimhan, 1985) to represent the naturally fractured reservoir was introduced to the history calculation phase, especially to incorporate the effect of reinjected water on the discharge enthalpies of production wells.

2. ONIKOBE RESERVOIR SYSTEM

Abe (1988) and Klein *et al.* (1990) provide a detailed description of the geological setting and the conceptual model of the field, summarized below. The field is located within the 2 million years old Onikobe caldera (about 8 km in diameter). The younger Katayama structural dome (3km x 2km) occupies the southeastern part of the caldera. A triangular topographic depression (1.5 km x 0.5 km) on top of the dome is interpreted to be a downfaulted block resulting from extensional stress across the top of the dome. The faults are believed to provide the vertical fluid conduits which charge the Onikobe geothermal reservoir.

The geology around the power station consists, in descending order, of the Katayama lacustrine deposit, the Ofukazawa andesite member of the Akazawa Formation, the Sannozawa Formation of Pleistocene, the Kanisawa Formation of Miocene, and Pre-tertiary granodiorite as the basement of the region. A two-phase geothermal reservoir is formed in the Ofukazawa andesite member made of andesite lava and tuff breccia shallower than 500 m in depth. The Sannozawa Formation made of altered dacitic tuff breccia has relatively low permeability. The Kanisawa Formation distributes in the depth from 700 m to 1,200 m, and a hot liquid reservoir is formed in the formation, especially in vertical fractures caused by a local horst structure with a temperature of around

250°C. (See Fig.2)

The temperature anomaly is centered on the Katayama area where the Onikobe geothermal power station is located, in the southeastern part of Onikobe caldera. The wellfield itself is quite small; the "project area" containing the wellheads and the power station occupies only 0.14 km^2. The early production wells produced a high-enthalpy mixture of water and steam from the shallow two-phase zone in the "project area". This steam production was not sustainable, however, and by 1980 utilization factor (=(Average Power through the year / Rated Output) x 100) of the plant had dropped below 50 % because of insufficient steam (Abe, 1993). Then, it was discovered that deeper wells, if deviation-drilled away from the center of the thermal anomaly, could also produce substantial quantities of hot liquid brines which were neutral or even slightly alkaline. Accordingly, starting in about 1982, production was shifted to these deeper, low-enthalpy wells. The deeper reservoir is a main production region of the Onikobe geothermal power station at present, and has been producing enough steam to sustain 12.5 MW power in this decade.

There are two types of production fluids in the fields, one is acid fluid with the pH of about 3, and the other is neutral to weak alkaline fluid with pH between 7 and 8. Klein *et al.* (1990) and Ajima *et al.* (1998) discussed these geothermal structure and chemistry.

3. NUMERICAL REPRESENTATION

A three-dimensional, two-phase numerical simulation model of the Onikobe fields was developed from available geological, hydrological, geophysical, geochemical and reservoir engineering data. The model was calibrated by numerous calculations, varying the various unknown parameters in the model, until a good match was obtained with both the natural-state (prior to the beginning of field operations in March 1975) conditions in the reservoir (mainly pressures and temperatures) and the fluid production history from the field during the 1975–1996 interval (mainly discharge enthalpies from the production wells). Numerical results discussed hereafter pertain to the final case.

The model covers 52 km^2 in the southern part of the Onikobe caldera, extending 8 km in the east-west direction and 6.5 km in the north-south direction (Fig.3). The spatial discretization is rather coarse with 11 grid blocks in the east-west direction ("i" index) and 10 blocks in the north–south direction ("j" index). Grid block dimensions vary between 0.3 and 2.0 km in the E – W direction and between 0.2 and 1.5 km in the N – S direction, with the highest resolution applied near the Onikobe borefield. Vertically the model extends from the earth surface (ranging from +200 m to +400 m above sea level – "ASL") to –2,000 m ASL. A total of 14 layers ("k" index) were used, with ten layers (each 200 m thick) between sea level and –2,000 m ASL, and four layers (each 100 m thick) above sea level. Some of the uppermost grid blocks are "void"; the total number of non-void blocks is 1,406. The total volume of these non-void blocks is 117 km^3.

The northern vertical boundary and the eastern vertical boundary were both treated as impermeable and insulated. By contrast, constant hydrostatic pressure boundary conditions were imposed on the southern and western grid boundaries. Pressures were also prescribed along the upper surfaces of the topmost grid blocks to permit vertical discharges and recharges of fluid and exchange of reservoir fluid with the shallow groundwater system. The bottom boundary of the computational volume was mainly treated as impermeable with a constant uniform upward heat flux (175 mW/m^2). Mass sources to represent the upwelling flow underlying the Katayama area were distributed in a restricted part of the bottom boundary. The spatial distribution, temperature and strength of these mass sources as well as permeability distribution throughout the system were used as the main fitting parameters in the natural-state simulation. A fixed uniform upward flux of hot (330°C) liquid water totaling 10 kg/s was finally imposed within a 2.25 km^2 area (-11.5 km E< x < -10 km E, -133.5 km N < y < -132 km N) as indicated in Fig.3.

Rock properties other than permeability (porosity, specific heat, thermal conductivity and density) used as input to the model were based on measured data for each rock type. Fig. 4 shows how the various major formations were assigned in the north-south section at "i = 6" and the east-west section at "j = 7". The values of the "bulk properties" of these formations were shown in Table 1. The distribution of the absolute permeability was established as a part of the "free parameter" variation process during the simulation. The final values are summarized in Table 2.

4. CALCULATION OF THE NATURAL STATE

The natural-state simulations were performed by the following two steps:

Step 1 :The calculations of the "natural state" (situation prior to human intervention) were carried out using the RANGER reservoir simulator (KCC, 1986). RANGER is restricted to single-phase liquid fluid flow, but has significant advantages in computational speed. Underground temperatures and pressures obtained after 100,000 years (relative to the initial state) were compared with measured values especially in the single-phase hot water region at medium to deep depth of the field, and the calculations were carried out until fairly good matches were obtained.

Step 2 :To take the two-phase region of the reservoir into account, the STAR general-purpose multiphase geothermal reservoir simulator (Pritchett, 1995) was used. Initial conditions for each STAR simulation were taken as the final values computed by RANGER, and the calculations were carried forward 2,000 years.

After a numerous natural-state calculations, reasonable matches were achieved between the observed and calculated subsurface temperature distributions. Fig. 5 is an example of the agreement between calculated and inferred temperature distribution at –300 m ASL. The figure shows that the

reasonable match was obtained on the whole, although the calculated temperature is about 20°C higher than observed one at the power station area. Fig.6 shows how the measured stable shut-in feedpoint pressures in the various Onikobe wells compare with values interpolated among principal grid-block pressures. The calculated pressures are, on the average, higher than observed ones - most of them were observed at mature condition -, but comparable with the values of the early exploration wells and wells located far away from the project area. The two-phase region was appeared at shallow blocks (k=12, 13 and 14) especially at neighborhood of the project area in the natural-state model. It also coincides with the conceptual model of the field.

5. WELL HISTORY MATCHING

Once a stable natural-state solution had been obtained, the history-match calculations were carried forward, imposing the known fluid production and injection histories based on field records of well flow rates for the period March 1975 – January 1997. The discharge enthalpies of the production wells were calculated by imposing the actual historical production and injection rates for each well in the appropriate grid blocks, as time-dependent sources and sinks of fluid mass, then compared with the observed enthalpies.

MINC (Multiple Interacting Continua) scheme (Pruess and Narasimhan, 1985; Pritchett, 1995) to represent the naturally fractured reservoir was introduced to these history calculations, with equivalent steady properties. In addition to be treated as a heterogeneous "porous medium", the various rock formations were treated as double-porosity "fractured media" within a region surrounding the Onikobe wellfield (-12 km E < x < -9 km E, -131.5 km N < y < -134 km N; total 7.5 km^2). The region treated using MINC is indicated in Fig. 3. The MINC technique permits improved representation of well discharge enthalpies for wells producing two-phase water/steam mixtures from the formation having the so-called "excess enthalpy". MINC subdivides the geological material into a small-volume, high-transmissivity "fracture zone" and a large-volume, low-transmissivity "matrix region" which is further subdivided into numerous sub-blocks to permit the explicit treatment of heat and mass transfer between the matrix region and the fracture zone. For the present study, the representative "matrix regions" were each subdivided into 8 sub-blocks, the average fracture separation (λ) is taken to be 50 m and 100 m, and the absolute permeability of the matrix region was taken as 0.5 microdarcies. The resulting global permeabilities of the fracture/matrix system were equivalent to steady properties.

Fig.7 is a map of the main wellfield of the Onikobe, including the location of abandoned wells. To represent the (average) enthalpy changes of shallow wells, we treated the groups of shallow production wells classified by steam flow pipe lines in which hot water flow rates were measured collectively; K-line wells that involved well 101, 102, 103 and 111, Z-line wells that involved well 104, 105, 106, 120 and 123, and WY-line wells that involved well 108, 112, 117 and 118. Figures 8 and 9 are examples of the enthalpy history matches for these shallow reservoir wells. Figures 10 and 11 present the cases of wells producing from the deep reservoir. The enthalpy declines observed in shallow production wells were reproduced in the simulation, as shown in Figures 8 and 9. The calculated enthalpies for some of the deep wells, however, were higher than the observed one, as exemplified by Fig. 11. Although there are still some discrepancies between the calculated and observed values in detailed viewing, these figures show that the comparisons between the calculated values by the model and the observed ones are, on the whole, reasonably satisfactory.

Fig.11 shows the changes in the discharge enthalpies of well 131, which is located in front of the southern reinjection well field, including the injection wells of I-4, I-5 and I-6. The observed changes in discharge enthalpy from the well exhibit the effects of cold reinjected water from nearby injection wells on the production well. The values calculated by the model using MINC treatment with a fracture spacing of 100 m show the same temporal trend as observed enthalpies, although calculated values were slightly higher. The figure suggests that the fracture separation of the reservoir system in the region around the southern reinjection area may be around 100 m.

The results of calculation forecasting the future response of the reservoir for an additional ten years (from January 1997 to January 2007) were also shown in Figures 8 - 11, assuming that well flow rates remained fixed after 1997. The figures suggest that the future performance of the well could be reasonably forecasted, although further refinement of the model with finer grid discretization seems to be essential, since the matchings between calculated and observed values were not completely attained in both natural-state and exploitation calculations.

6. CONCLUDING REMARKS

A numerical model has been constructed for the Onikobe geothermal field, which is internally consistent and in comparably good agreement with available measurements from the field. The steady "natural" state model of the field was developed by a natural state simulation. After the natural state model was derived, a further calibration of the model was carried out by matching the known and calculated enthalpy histories of the existing wells. MINC formulation to represent the naturally fractured reservoir was used in these history calculations, with equivalent steady properties. The enthalpy declines observed in shallow production wells as well as the thermal effects of reinjected water on the deep production well were reproduced in the simulation. These calculations indicate that the average fracture spacing of the reservoir near the southern reinjection area was around 100m. The further refinement of the model attaining more complete matches between the observed and calculated values will be needed to provide more accurate forecasting of reservoir performance.

ACKNOWLEGEMENTS

The authors wish to thank the management of the Electric

Power Development Company, Ltd. (EPDC) for the permission to publish this paper. They would also like to thank H. Muratake of Kaihatsu Computing Service Center, Ltd. (KCC) for his generous help in this study.

REFERENCES

Abe, M. (1988). Onikobe Geothermal Power Plant. In: *Geothermal Fields and Power Plants in Japan*, International Symposium on Geothermal Energy, Kumamoto and Beppu, Japan, pp.49-56.

Abe, M. (1993). Long term use of acidic reservoir at Onikobe geothermal power plant. *Proceedings 15th New Zealand Geothermal Workshop*, pp.5-10.

Ajima, S., Todaka, N., and Muratake, H. (1998). An interpretation of smectite precipitation in production wells caused by the mixing of different geothermal fluids. *Proc. Twenty-Third Workshop on Geothermal Reservoir Engineering*, Stanford University, Stanford, California, pp.264-269.

KCC (1986). *Report on the EPDC research project on the development of the geothermal reservoir simulator.* Report for the EPDC, Tokyo. (in Japanese)

Klein, C.W., McNitt, J.R., Sanyal, S.K., Abe, M., and Nakanishi, S. (1990). Corrosion vs. temperature: Field development options at Onikobe geothermal field, Miyagi prefecture, Japan. *Geothermal Resources Council Transactions*, Vol.14, Part II, pp. 1493-1499.

Pritchett, J.W. (1995). STAR: A geothermal reservoir simulation system, *Proc. World Geothermal Congress 1995*, Florence, Italy, pp. 2959-2963.

Pruess, K. and Narasimhan, T.N. (1985). A practical method for modeling fluid and heat flow in fractured porous media. Soc. Pet. Eng. J., February, pp. 14-26.

Sanyal, S.K., Antunez, E.U., Abe, M., and Nakanishi, S. (1990). Numerical modeling of a mature, high temperature geothermal reservoir: A case history from the Onikobe field, Miyagi prefecture, Japan. *Geothermal Resources Council Transactions*, Vol.14, Part II, pp. 1339-1345.

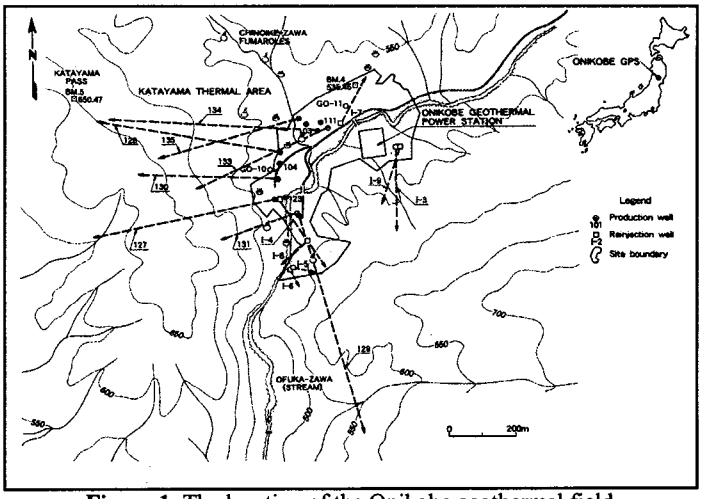

Figure 1. The location of the Onikobe geothermal field.

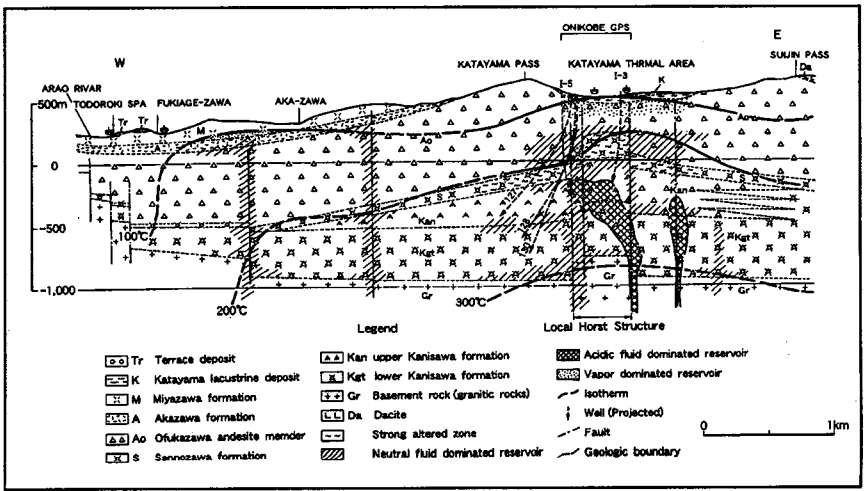

Figure 2. A schematic east-west stratigraphic and temperature cross section of the Onikobe geothermal system.

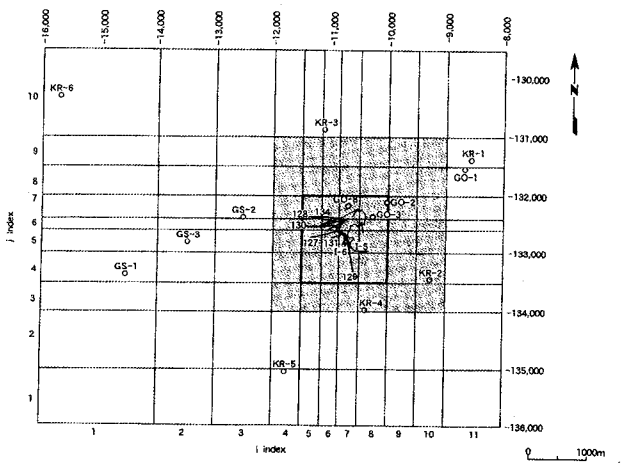

Figure 3. Areal view of the computational grid. Square of solid line is the region of deep hot water inflow. Shaded area uses the "MINC" double-porosity representation. Elsewhere, the system is treated as a porous medium.

Table 1. Bulk properties of geological formations in simulation model.

FORMATION	FORMATION POROSITY	PROPERTIES OF ROCK GRAIN MATERIALS		
		Mass Density (g/cm³)	Thermal Conductivity (W/m-°C)	Heat Capacity (J/g-°C)
Quaternary sediments	8%	2.2	1.82	1
Quaternary dacite	9%	2.2	1.59	1
Miyazawa pyroclastics	18%	2.1	0.75	1
Akazawa pyroclastics	21%	2.2	0.71	1
Pleistocene sediments	11%	2.1	2.40	1
Pleistocene andesite	10%	2.4	1.34	1
Pliocene pyroclastics	30%	2.2	1.34	1
Miocene andesite	15%	2.6	2.01	1
Miocene sediments	11%	2.1	2.60	1
Miocene pyroclastics	10%	2.6	2.76	1
Pre-tertiary basement	2%	2.7	2.60	1

Table 2. Permeabilities of the various geological formations in simulation model

FORMATION	ABSOLUTE FORMATION PERMEABILITY (MILLIDARCIES)					
	East-West		North-South		Vertical	
	minimum	maximum	minimum	maximum	minimum	maximum
Quaternary sediments	20	20	15	15	0.1	0.1
Quaternary dacite	5	5	0.05	0.05	0.01	0.01
Miyazawa pyroclastics	0.05	5	0.0375	5	0.0005	0.25
Akazawa pyroclastics	0.25	5	0.25	5	0.005	15
Pleistocene sediments	20	20	0.5	0.5	5	5
Pleistocene andesite	0.1	5	0.1	5	0.005	1.5
Pliocene pyroclastics	2.5	20	1	20	0.005	20
Miocene andesite	1.5	20	1	20	0.05	20
Miocene sediments	0.01	10	0.05	0.5	0.005	0.005
Miocene pyroclastics	0.0075	15	0.0075	25	0.005	10
Pre-tertiary basement	0.005	5	0.005	5	0.005	5

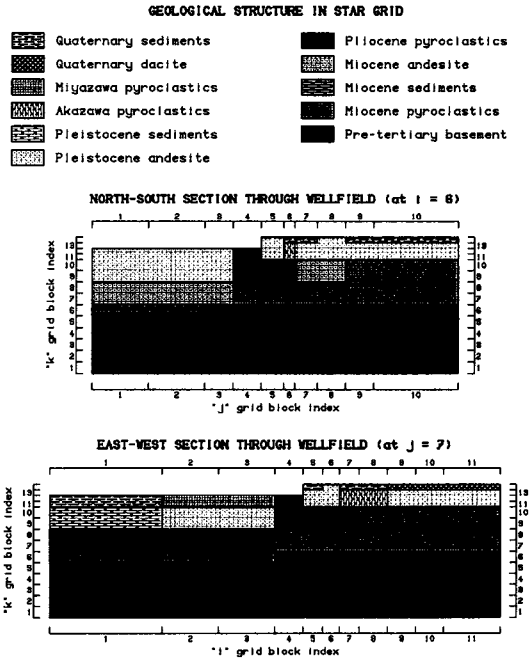

Figure 4. Assignment of geological formations to grid blocks in vertical planes passing through the wellfield.

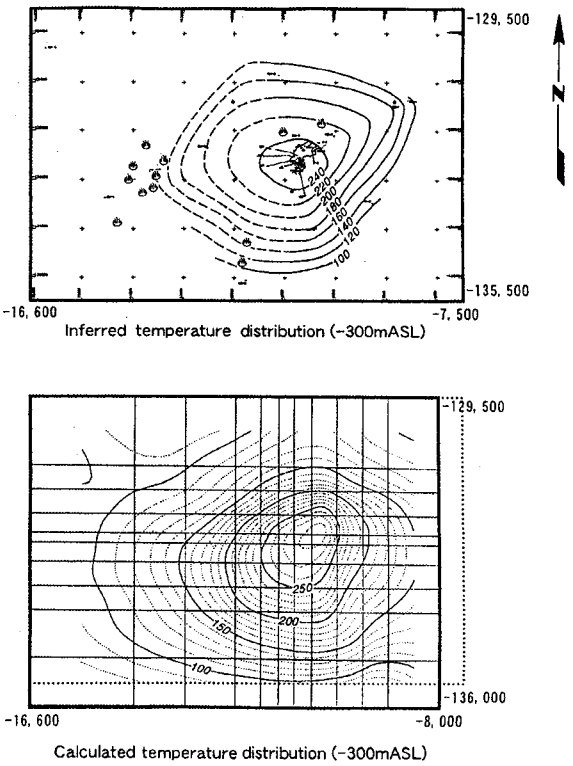

Figure 5. Comparison between inferred temperature distribution (upper) and calculated temperature distribution (lower) at –300m ASL. Dotted lines show the extent of the upper figure.

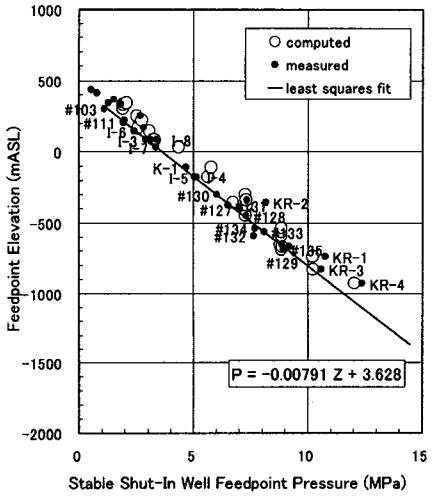

Figure 6. Comparison of measured and computed reservoir pressure. Straight line is a correlation of measured pressure with feedpoint elevation. "KR" series wells and early exploratory wells are not included in the correlation.

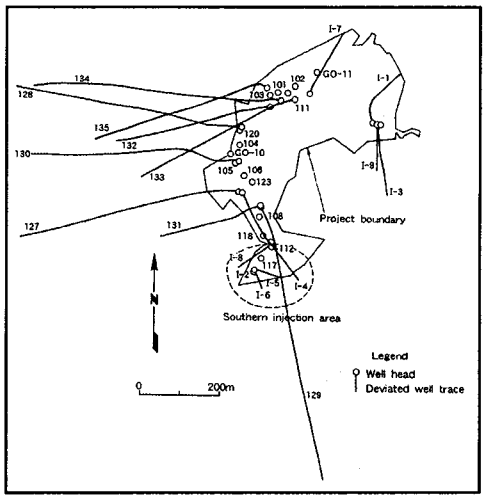

Figure 7. Location of wells including abandoned wells

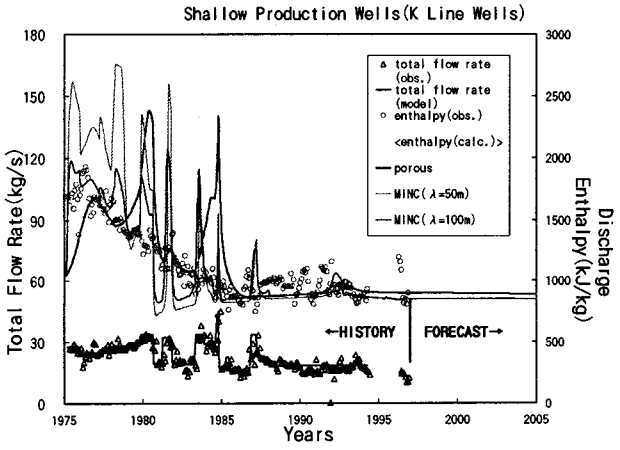

Figure 8. Enthalpy matching and imposed actual production flow rate, shallow K-Line wells (well 101, 102, 103 and 111).

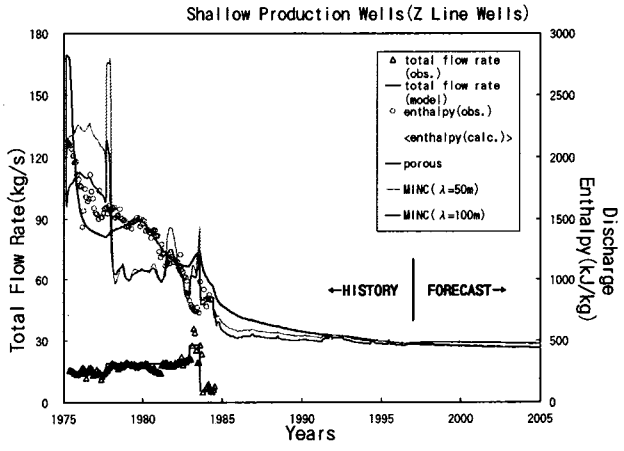

Figure 9. Enthalpy matching and imposed actual production flow rate, shallow Z-Line wells (well 104, 105, 106, 120 and 123).

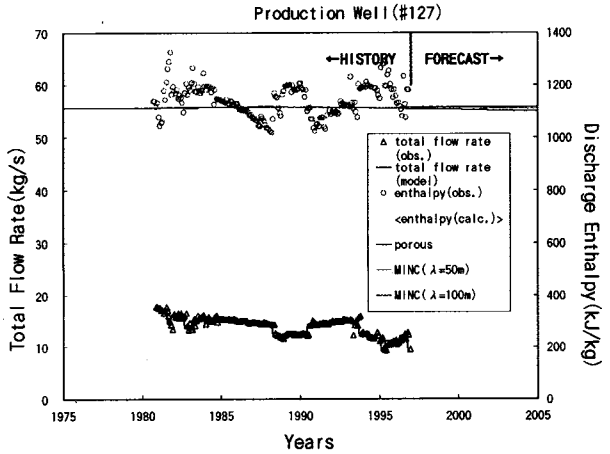

Figure 10. Enthalpy matching and imposed actual production flow rate, well 127.

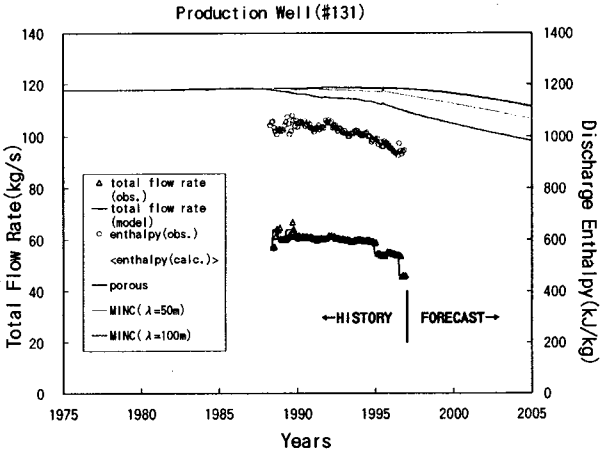

Figure 11. Enthalpy matching and imposed actual production flow rate, well 131.